Chemical Engineering Science 66 (2011) 3531–3539

Contents lists available at ScienceDirect

Chemical Engineering Science

journal homepage: www.elsevier.com/locate/ces

A general rate model approach for the optimization of the core radius fraction for multicomponent isocratic elution in preparative nonlinear liquid chromatography using cored beads

Tingyue Gu [a,*], Mingqing Liu [a], Kwok-Shun C. Cheng [b], Senthilkumar Ramaswamy [b], Chen Wang [b]

[a] Department of Chemical and Biomolecular Engineering, Ohio University, Athens, OH 45701, USA
[b] BioProcess R&D, Millipore Corporation, 80 Ashby Road, M1 North, Bedford, MA 01730, USA

ARTICLE INFO

Article history:
Received 31 December 2010
Received in revised form
28 February 2011
Accepted 16 April 2011
Available online 22 April 2011

Keywords:
Chromatography
Mass transfer
Mathematical modeling
Optimization
Cored beads
Pellicular particles

ABSTRACT

Cored beads (also known as pellicular, superficially porous, and fused-cored beads or particles) offer advantages over fully porous beads in reduced diffusional mass transfer resistances in particle macropores and separation times in liquid chromatography (LC). They are also used to regulate bead densities. The core of a bead has a relatively small volume and yet presents a large linear distance for diffusional mass transfer inside particle macropores. Using a non-porous inert core, intraparticle diffusional mass transfer resistance can be reduced with a relatively small loss in binding capacities. In multicompnent isocratic elution chromatography, cored beads are a compromise between fully porous beads and non-porous beads. Non-porous beads completely eliminate intraparticle diffusion, providing sharp elution peaks with the shortest retention times. However, they do not provide a sufficient retention time range for peaks to separate in preparative LC because of their limited binding capacities. At the other end, fully porous beads offer the largest retention time differences, but suffering from excessive band broadening. For a particular multicomponent elution system, core radius fraction can be optimized to take the advantages of both fully porous beads and non-porous beads. This work presented a general rate model for cored beads and its numerical solution strategy. The model considered axial dispersion, interfacial mass transfer, intraparticle diffusion, and multicomponent Langmuir isotherm. Computer simulation was used to study the effects of core radius fraction on breakthrough curves and elution peaks. The model was used to optimize the core radius fraction for a preparative ternary elution system as an example case.

1. Introduction

In liquid chromatography (LC), eluites must migrate from the bulk-liquid phase to the particle phase by crossing a stagnant liquid film surrounding each particle. This is the so-called interfacial film mass transfer. Inside the particle macropores, diffusion in the stagnant liquid allows eluites to interact with the binding sites. The core section of a fully porous bead offers a disportionately small volume that corresponds to a small percentage of binding sites, but it presents a relatively large linear radial distance for diffusional mass transfer (Kirkland et al., 2000). Non-porous beads have been a success in analytical LC because they provide sharp peaks and fast separation times (Lee, 1997; Rissler, 2000; Xiang et al., 2003; Fekete et al., 2010). However, these beads do not offer sufficient binding sites for peak separations in preparative LC (Kirkland et al., 2000; Miyabe, 2008). Fully porous and non-porous beads offer two extreme cases for mass transfer and binding capacities. The former offers the largest binding capacities and diffusional intraparticle mass transfer resistance, while the latter the smallest binding capacities and complete elimination intraparticle mass transfer. In preparative- and large-scale LC, a substantial binding capacity is needed to create retention time differences among peaks. However, with fully porous beads, band broadening makes baseline separation difficult when the peaks migrate inside the column for too long. Between fully porous and non-porous beads, there is a middle ground that is better for many systems.

Cored beads (Wang et al., 2007) are a compromise between fully porous and non-porous beads. Fig. 1 is a sketch of a spherical cored bead. Cored beads are also known as pellicular (Coutinho et al., 2001; Zhou et al., 2004; Greibrokk, 2004), superficially porous (Kirkland et al., 2000), and fused-core (Manchon et al., 2010) beads or particles. Fig. 2 shows the theoretical relationships of core radius fraction with core volume fraction and shell volume

* Corresponding author. Tel.: +1 740 593 1499; fax: +1 740 593 0873.
E-mail address: gu@ohio.edu (T. Gu).

0009-2509/$ - see front matter © 2011 Elsevier Ltd. All rights reserved.
doi:10.1016/j.ces.2011.04.021

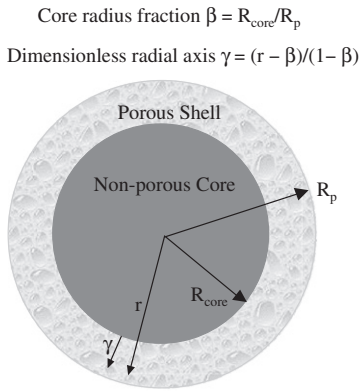

Fig. 1. Schematic of a spherical cored bead with an inert non-porous core and a porous shell.

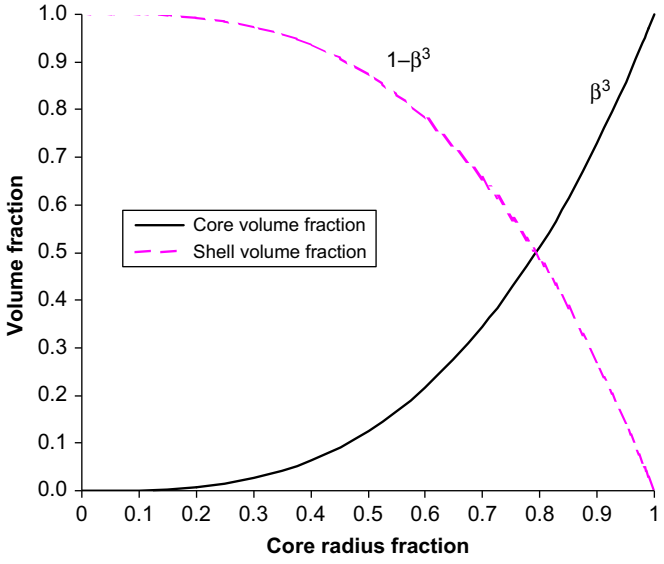

Fig. 2. Theoretical core volume and shell volume distributions as functions of core radius fraction (β).

fraction. The dashed curve in Fig. 2 indicates that the porous shell volume (including macropores) declines very slowly initially following the increase of core radius fraction before the core radius fraction reaches around 0.5.

Cored beads can be made nearly perfectly spherical with a narrow particle size distribution using suitable cores such as borosilica beads (Wang et al., 2007). This kind of spherical beads can reduce non-ideal flow inside a column. They also yield a lower column pressure drop compared to beads with smaller particle sizes (Kirkland et al., 2000; Fanigliulo et al., 2010; Pietrogrande et al., 2010). Cored beads have been used in various LC separations, especially in ion exchange (Horvath et al., 1967; Pesek and Frost, 1973; Ning et al., 1998; Wang et al., 2007). They have been used for separations of proteins and peptides (Kirkland et al. 2000; Zhou et al., 2007; Kiss et al., 2010) including proteins in proteomic research (Wang, et al., 2006), nucleotides (Horvath et al., 1967), and other compounds (Ning et al., 1998). Cabooter et al. (2010) and Fanigliulo et al. (2010) compared several commercially available fully porous and cored beads experimentally. Cored beads have also been used in gas chromatography according to Kirkland (1969).

Cored beads have a special niche in expanded bed operations because the cores allow the control of bead density through the use of cores with different densities including stainless steel cores (Palsson et al., 2000; Zhou et al., 2004). Ding and Sun (2005) fabricated gel-coated cored beads with dense magnetic cores for protein separations in a magnetically stabilized fluidized bed. The use of a rigid core relieves bed compression for soft gels (Wang et al., 2007). This means during scale-up, cored beads allow longer columns that are better for peak resolution.

Yang and Hu (1996) derived the theoretical moment expressions for elution and frontal linear chromatography with pellicular ion exchange resins. Zhou et al. (2004) used a general rate model for cored beads to obtain intraparticle diffusion coefficients. They did not provide numerical methods or simulated concentration profiles. Kaczmarski and Guiochon (2007) studied thin-shelled coated beads with a lumped particle model assuming that the concentration profile inside the thin shell could be represented by a single averaged concentration value. To compare with fully porous beads that can have steep concentration changes, they used a standard general rate model for the fully porous beads. More recently, Li et al. (2010) performed optimization of core size for linear chromatography by minimizing height equivalent theoretical plate (HETP) number.

So far, in the open literature, there is no theoretical comparison of fully porous beads, cored beads, and non-porous beads in a systematic way to illustrate the principle of optimization of the core radius fraction for designing cored beads used in nonlinear preparative multicomponent isocratic elution. This work presented a general rate model for cored beads, which considered axial dispersion, interfacial film mass transfer, intraparticle diffusion, and multicomponent Langmuir isotherm. A theoretical three-component elution case study was carried out using the model to demonstrate the existence of an optimal core radius fraction for faster baseline separation.

2. Model and numerical methods

The following model equations describe mass transfer in the column bulk-fluid phase and in the stationary liquid phase inside particle macropores. Cored beads are assumed to have a uniform particle size (R_p) and core size (R_{core}). The inner core cannot be penetrated and there is only diffusion (no convection) in the porous shell. The column is assumed to be isothermal:

$$-D_{bi}\frac{\partial^2 C_{bi}}{\partial Z^2}+v\frac{\partial C_{bi}}{\partial Z}+\frac{\partial C_{bi}}{\partial t}+\frac{3k_i(1-\varepsilon_b)}{\varepsilon_b R_p}(C_{bi}-C_{pi,R=Rp})=0 \quad (1)$$

$$(1-\varepsilon_p)\frac{\partial C^*_{pi}}{\partial t}+\varepsilon_p\frac{\partial C_{pi}}{\partial t}-\varepsilon_p D_{pi}\frac{1}{R^2}\frac{\partial}{\partial R}\left(R^2\frac{\partial C_{pi}}{\partial R}\right)=0 \quad (2)$$

Multicomponent Langmuir isotherm can be expressed as

$$C^*_{pi}=\frac{a_i C_{pi}}{1+\sum_{j=1}^{N_c} b_j C_{pj}} \quad (3)$$

To reduce the number of variables, the PDE system is non-dimensionalized using the following dimensionless variables and parameters:

$$c_{bi}=C_{bi}/C_{0i}, c_{pi}=C_{pi}/C_{0i}, c^*_{pi}=C^*_{pi}/C_{0i}, r=R/R_p,$$
$$z=Z/L, Pe_{Li}=vL/D_{bi}, Bi_i=k_iR_p/(\varepsilon_p D_{pi}), \eta_i=\varepsilon_p D_{pi}L/(R_p^2 v),$$
$$\xi_i=3Bi_i\eta_i(1-\varepsilon_b)/\varepsilon_b, \tau=vt/L$$

Eqs. (1)–(3) can be transformed into dimensionless forms as follows:

$$-\frac{1}{Pe_{Li}}\frac{\partial^2 c_{bi}}{\partial z^2}+\frac{\partial c_{bi}}{\partial z}+\frac{\partial c_{bi}}{\partial \tau}+\xi_i(c_{bi}-c_{pi,r=1})=0 \quad (4)$$

$$(1-\varepsilon_p)\frac{\partial}{\partial \tau}c^*_{pi}+\varepsilon_p\frac{\partial c_{pi}}{\partial \tau}-\eta_i\frac{1}{r^2}\frac{\partial}{\partial r}\left(r^2\frac{\partial c_{pi}}{\partial r}\right)=0 \quad (5)$$

in which stationary phase eluite concentrations c_{pi}^{*} can be calculated using the local eluite concentrations in the fluid inside the particle macropores (c_{pi}) from the following dimensionless multicomponent Langmuir isotherm:

$$c_{pi}^{*}=\frac{a_i c_{pi}}{1+\sum_{j=1}^{N_s}(b_j C_{0j})c_{pj}} \tag{6}$$

Apart from adsorption chromatography, the Langmuir isotherm sometimes also finds its use in ion-exchangers for protein separations (Misak, 1993). The isotherm can be readily substituted with other types of isotherms for the general model.

For fully porous beads, the r-axis in Eq. (5) ranges from 0 to 1. While for cored beads, it ranges from R_{core}/R_p to 1. In order to use the model to study cored beads with any core radius fraction denoted $\beta(=R_{core}/R_p)$, it is essential to allow the core radius to be varied. For cored beads in Eq. (5), $\beta\le r\le 1$. $\beta=0$ corresponds to fully porous beads. Because the r-axis does not start from zero for cored beads, it is inconvenient for the implementation of the orthogonal collocation method that is designed for a linear distance ranging from 0 to 1. Thus, it is necessary to substitute it with a dimensionless γ-axis (Fig. 1), such that $0\le\gamma\le 1$, where

$$\gamma=\frac{r-\beta}{1-\beta} \tag{7}$$

Inserting $r=\gamma(1-\beta)+\beta$ into Eq. (5) yields

$$(1-\varepsilon_p)\frac{\partial}{\partial\tau}c_{pi}^{*}+\varepsilon_p\frac{\partial c_{pi}}{\partial\tau}-\eta_i\left[\frac{1}{(1-\beta)^2}\frac{\partial^2 c_{pi}}{\partial\gamma^2}+\frac{2}{\gamma(1-\beta)+\beta}\cdot\frac{1}{1-\beta}\frac{\partial c_{pi}}{\partial\gamma}\right]=0 \tag{8}$$

The following initial and boundary conditions are needed for the general rate model:

Initial conditions: At $\tau=0$, $c_{bi}=c_{bi}(0,z)=0$, $c_{pi}=c_{pi}(0,r,z)=0$.

Boundary conditions:

At $z=0$,

$$\partial c_{bi}/\partial z=Pe_{Li}[c_{bi}-C_{fi}(\tau)/C_{0i}] \tag{9}$$

and at $z=1$,

$$\partial c_{bi}/\partial z=0. \tag{10}$$

At $\gamma=0$,

$$\partial c_{pi}/\partial\gamma=0 \tag{11}$$

and at $\gamma=1$,

$$\partial c_{pi}/\partial\gamma=Bi_i(c_{bi}-c_{pi,r=1}) \tag{12}$$

For breakthrough analysis, the dimensionless feed concentration profile $C_{fi}(\tau)/C_0=1$ is maintained. For elution, $C_{fi}(\tau)/C_0=1$ during $0\le\tau\le\tau_{imp}$ and $C_{fi}(\tau)/C_0=0$ for $\tau>\tau_{imp}$, where τ_{imp} is the dimensionless sample injection time for a rectangular pulse sample.

The PDE system consisting of Eqs. (4) and (8) were solved numerically. The finite element method was used to discretize the z-axis in Eq. (4) as shown by Gu (1995). The first- and second-order derivatives with respect to γ in Eq. (8) were discretized using orthogonal collocation with the general purpose A, B matrices (not the A, B matrices for spherical particles), respectively (Finlayson, 1980) for interior collocation points. The A and B matrices were calculated using the polynomial roots and formulas provided on Page 77 in the book by Finlayson (1980). The orthogonal collocation method also needed two exterior collocation points, one at the core surface and the other on the bead surface, which were calculated from the boundary conditions at $\gamma=0$ and $\gamma=1$, respectively. At the bead surface ($\gamma=1$) and the core surface ($\gamma=0$), discretizations of Eqs. (12) and (11) led to the following two expressions for the calculations of eluite concentrations in the fluid inside macropores at these two locations using the matrix A and eluite concentrations in the fluid inside the macropores at the interior collocation points, respectively:

$$c_{pi,\gamma=1}=\frac{A_{N+2,1}\sum_{j=2}^{N+1}A_{1,j}(c_{pi})_j-A_{1,1}\sum_{j=2}^{N+1}A_{N+2,j}(c_{pi})_j+A_{1,1}(1-\beta)Bi_i c_{bi}}{A_{1,1}(1-\beta)Bi_i-A_{N+2,1}A_{1,N+2}+A_{1,1}A_{N+2,N+2}} \tag{13}$$

$$c_{pi,\gamma=0}=-\frac{1}{A_{1,1}}\left(\sum_{j=2}^{N+1}A_{1,j}(c_{pi})_j+A_{1,N+2}c_{pi,\gamma=1}\right) \tag{14}$$

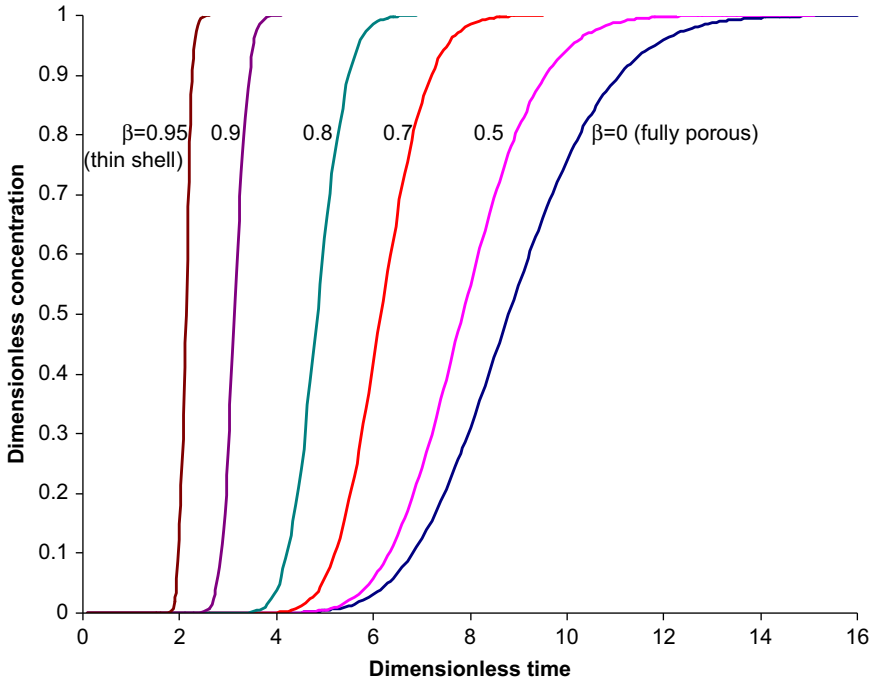

Fig. 3. Effect of core radius fraction on a breakthrough curve. Parameters used in the simulation are listed in Table 1.

This implementation of the orthogonal collocation method for the cored bead model differed from that for fully porous beads described in detail by Gu (1995), because the latter needs only one exterior collocation point at the outer surface and it uses the A, B matrices for the spherical geometry (Finlayson, 1980). It is significantly more complicated for cored beads than for fully porous beads. However, it is necessary because this solution allows the study of cored beads with any core radius fraction. If a lumped particle model is used, the model will be accurate for thin-shelled cored beads, but inadequate for large beads with smaller cores, because the concentration profiles inside the porous shell need to be described with several discretization points.

After discretizing the γ-axis using the orthogonal collocation method, and z-axis using exactly the same finite element method as detailed by Gu (1995) for a column packed with fully porous beads, Eqs. (4) and (5) together with Eq. (6) yielded a first-order ordinary differential equation (ODE) system that was solved using an efficient public domain ODE solver called VODE by Brown et al. (1989). The Fortran computer language was used to implement the numerical solution. It was linked to a graphical user interface written in C++ computer language.

3. Results and discussion

3.1. Effect of core radius fraction (β) on breakthrough time and curve stiffness

Fig. 3 shows a comparison of the breakthrough curves for different core radius fractions and for fully porous beads for a single-component system. Parameters used in simulation are listed in Table 1. As β increased from 0 (fully porous beads) to 0.95 (beads with a very thin shell), the breakthrough curves became sharper and took off earlier. The sharper breakthrough curves were due to reduced intraparticle diffusional mass transfer resistance and also a shorter breakthrough time. A shorter breakthrough time allowed less time for a breakthrough curve to diffuse inside the column. Because cored beads produce sharper breakthrough curves as β increases, these curves with different β values will never cross over. Thus, cored beads have a lower loading capacity for complete or partial breakthrough compared with fully porous beads.

The column hold-up capacity at breakthrough leveling off for an eluite accounts for the amount of the eluite trapped in the bed voids between beads, in the particle macropores and in the

Table 1
Parameters used for computer simulation.

Figure number	Species number	Dimensionless physical parameters							Numerical parameters	
		Pe	η	*Bi*	ε_b	ε_p	*a*	bC_0	*Ns*	*N*
3	1						10	0.5×0.1		
4	1						10	0.5×0.1		
	1	1500	2	50	0.4	0.5	10	0.5×0.1	10–30[a]	2
5–8	2						30	1.5×0.4		
	3						70	3.5×0.4		

[a] Sharper concentration profiles required a larger number of finite elements and a longer CPU time in order to eliminate any oscillation due to curve stiffness.

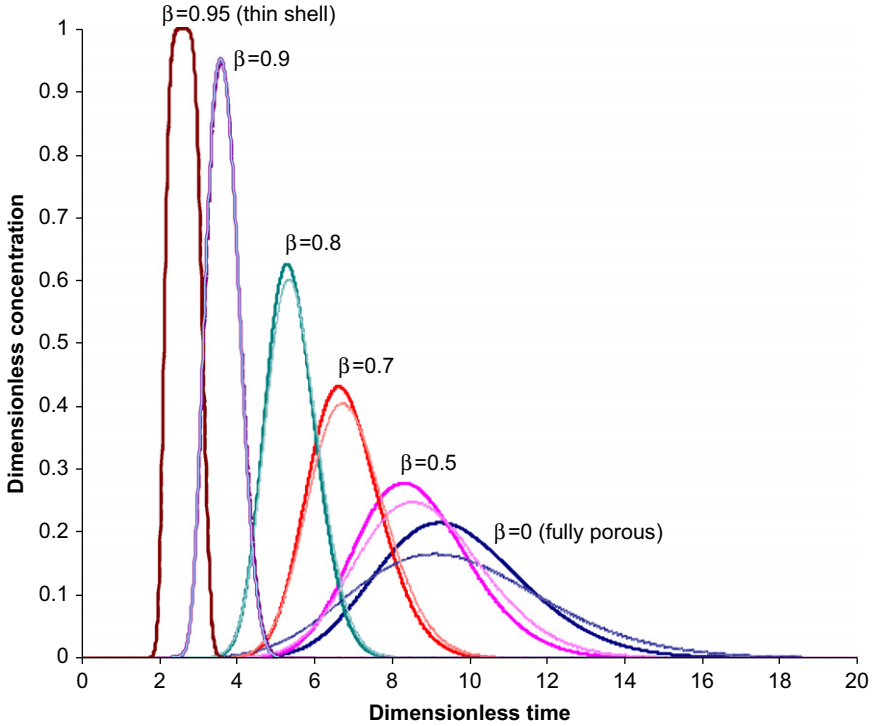

Fig. 4. Effect of core radius fraction (β) on preparative isocratic elution. Parameters used in the simulation were the same as Fig. 3, but with a sample pulse size of one in dimensionless time. Solid lines used two interior collocation points ($N=2$) and dashed lines used only one ($N=1$) in computer simulation.

stationary phase (due to binding). The dimensionless column hold-up capacity corresponds to a capacity area (CA) in a dimensionless breakthrough curve (Gu, 1995) that is bordered by the x- and y-axes, the breakthrough curve and the horizontal breakthrough leveling off line. A simple mass balance on a breakthrough curve yields the following equation for the calculation of CA:

$$CA = 1 + \frac{1}{\varepsilon_b}(1-\beta^3)\left[(1-\varepsilon_b)\varepsilon_p + (1-\varepsilon_b)(1-\varepsilon_p)\frac{a}{1+bC_0}\right] \quad (15)$$

in which $(1-\beta^3)$ is volume fraction (including particle macropores) of the porous shell that has binding sites. As β increases, CA decreases due to loss of particle macropore volume and binding capacity. In Fig. 3, the theoretical CA values calculated from Eq. (15) for the six breakthrough curves (β=0, 0.5, 0.7, 0.8, 0.9, and 0.95) were 8.8929, 7.9063, 6.1856, 4.8517, 3.1390, and 2.1257, respectively. The corresponding CA values from integrating the simulated breakthrough curves in Fig. 3 were found to be 8.8924, 7.9062, 6.1854, 4.8516, 3.1389, and 2.1258, respectively, all within 0.01% of their corresponding theoretical value. This is a partial indication of the accuracy of the numerical methods used in this work.

3.2. Effect of core radius fraction (β) on peak retention time and band broadening in elution

Fig. 4 shows that the single-component peak became sharper with a smaller retention time as β increased. The parameters used for Fig. 4 were the same as those for Fig. 3 (see Table 1), except that Fig. 4 shows elution instead of breakthrough. The sample pulse size for Fig. 4 was one in dimensionless time, equivalent to a sample volume of $V_b\varepsilon_b$, or 40% of column volume because ε_b=0.4 was used in the simulation. This kind of sample size is preparative for isocratic elution. The Pe, η values in Table 1 are relatively large that often result in rather sharp peaks, representing higher resolution columns due to good mass transfer (Gu, 1995). They are likely achieved by columns packed with relatively rigid smaller beads instead of larger beads with thick soft gel shells that usually do not provide high peak resolutions.

Fig. 4 correlates very well with the stiffness and take-off times of the breakthrough curves in Fig. 3. The shorter retention times were due to an increased loss of binding sites with a larger β value. Loss of binding sites resulted in less interaction between the eluite and the stationary phase for adsorption and dissociation. The sharper and more symmetric peaks in Fig. 4 were due to reduced intraparticle diffusional mass transfer resistance and also shorter retention times. The flat top of the β=0.95 peak means that it actually achieved breakthrough leveling off due to a sample overload for such a low capacity column packed with cored beads with a very large β.

In Fig. 4, the solid curves were simulated using two interior collocation points (N=2). Using N=3 (not plotted in Fig. 4) did not provide any significant differences compared with N=2. This meant that N=2 was sufficient for convergence of results. The dashed curves were obtained using N=1, which resulted in more

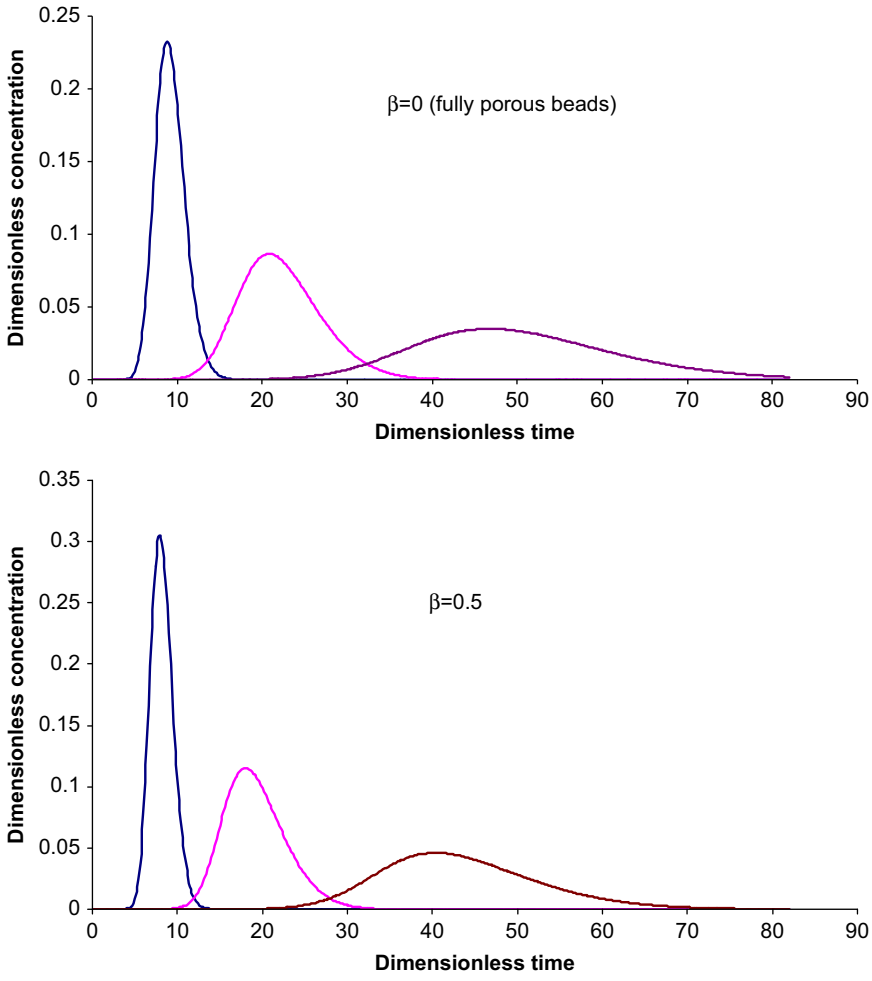

Fig. 5. Comparison of fully porous beads with cored beads with a small radius fraction (β=0.5) in isocratic elution of a three-component system and a sample pulse size of one in dimensionless time.

diffused peaks for the four peaks with $\beta < 0.9$. This indicated that with $N=1$, three collocation points (one interior collocation point plus two exterior collocation points at the core surface and particle surface, respectively) were not sufficient to describe the rather complicated concentration profiles inside the particle macropores when the shell was not thin enough. For high accuracies in simulation results, a minimum of $N=2$ should be used for beads with a significant shell thickness. Fig. 4 shows that, for $\beta=0.9$ and 0.95, the differences between the solid and the dashed curves were hardly noticeable. This means that $N=1$ was sufficient to describe the simple eluite concentration profile in the particle macropores for thin-shelled cored beads.

3.3. Optimization of core radius fraction (β) in multicomponent elution

Figs. 5–7 demonstrate the effect of β on retention times and band broadening on the isocratic elution of a preparative three-component system. Parameters used in the simulation are listed in Table 1. The three peaks had a fairly large preparative sample pulse size of one in dimensionless time, equivalent to a sample volume of 40% of the column volume as in Fig. 4. Fig. 5 shows that fully porous beads provided the largest retention time differences and most severe band broadening. It did not achieve a baseline separation of the three peaks. Cored beads with $\beta=0.5$, corresponding to a shell volume fraction of 87.5%, did not make much improvement in separation time and peak resolution. As β values increased to 0.8 and 0.9, peaks became much sharper (Fig. 6). With $\beta=0.8$ and 0.9 (Fig. 6), baseline separation of the three peaks was achieved because of reduced band broadening even though the retention time differences were much smaller compared to those in fully porous beads (Fig. 5). The total dimensionless time needed for completely eluting out the three peaks was approximately 80 for fully porous beads (Fig. 5), compared with 20 for cored beads having $\beta=0.9$, which corresponds to 27% porous shell volume fraction (Fig. 6). The latter was 4 times faster and better in separation results, i.e., sharper peaks and baseline separation.

When β further increased to 0.96 (Fig. 7), peaks became even sharper and the total dimensionless run time to elute out the three peaks was only 9. The retention time differences were so small that there was simply not enough room for the three peaks to achieve baseline separation. The first peak for $\beta=0.9$ in Fig. 6, and the first and second peaks for $\beta=0.96$ in Fig. 7 all had a peak-top concentration higher than the dimensionless feed concentration of one. This phenomenon can be explained by the so-called displacement effect (Gu et al., 1990) under the column overload condition. It is very interesting to note that the peak-top concentration for the first peak for $\beta=0.9$ in Fig. 6 was much higher than one, while a baseline separation was achieved in isocratic elution. This would be quite desirable if the first peak was the product peak. In this case, without the displacement effect exerted by the second and third eluites, the peak concentrating

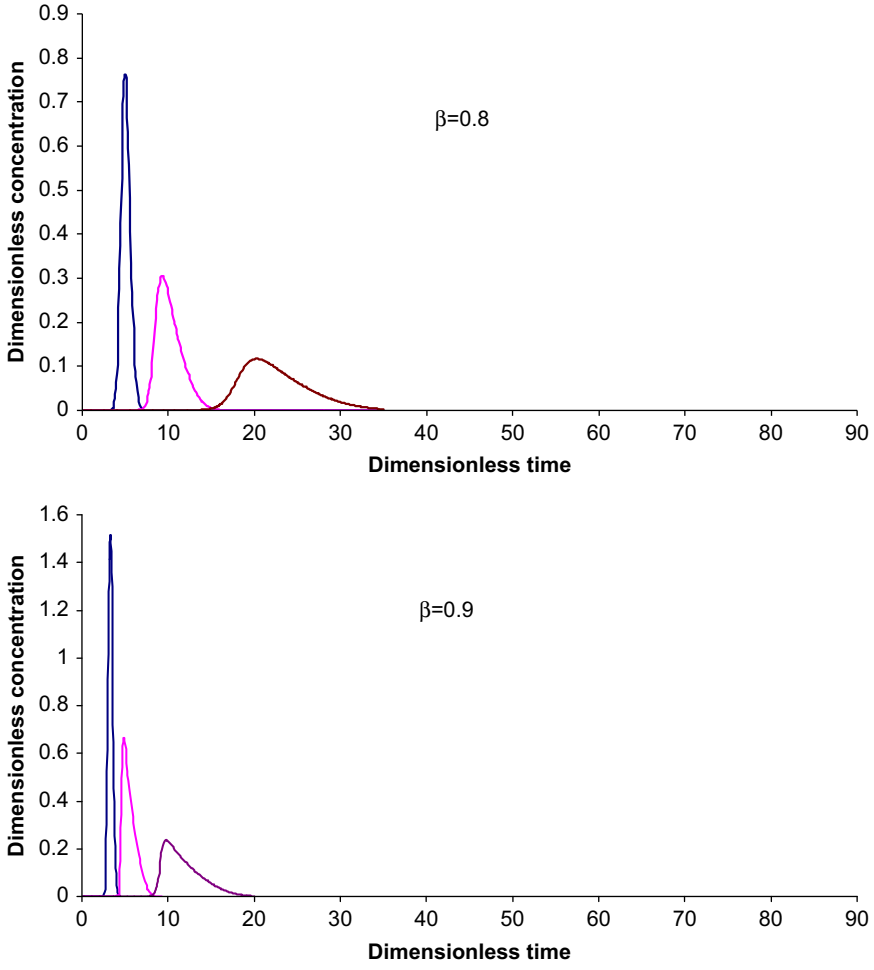

Fig. 6. Optimization of core radius fraction to achieve faster baseline separation with a sample pulse size of one in dimensionless time. Both $\beta=0.8$ and $\beta=0.9$ achieved baseline separation with the latter significantly faster.

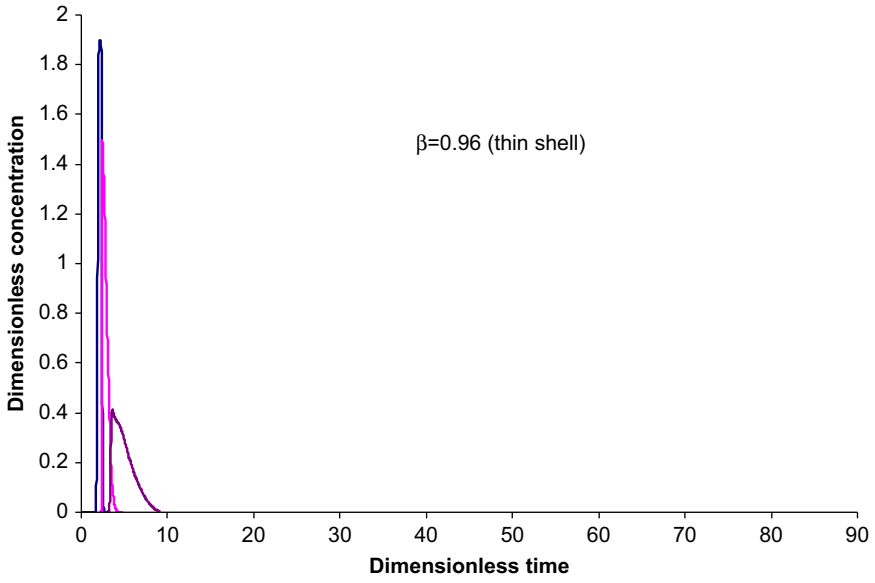

Fig. 7. Effect of a very large core radius fraction (β=0.96) on preparative-scale elution with a sample pulse size of one in dimensionless time.

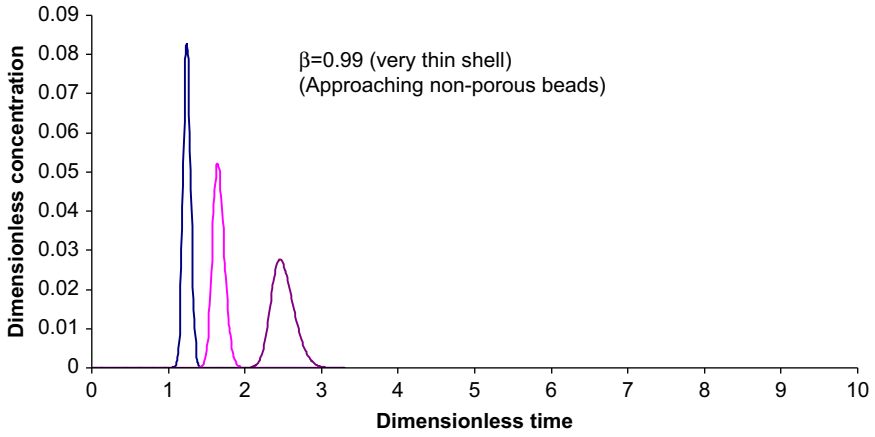

Fig. 8. Baseline separation with a very large core radius fraction of β=0.99 and a very small sample pulse size of 0.01 in dimensionless time (analytical-scale elution). The *x*- and *y*-axes were enlarged to show details compared to Fig. 7.

effect for the first eluite would never happen in isocratic elution. This argument is supported by the β=0.9 peak in Fig. 4 in a single-component elution.

Should a β value larger than 0.96 be used for the ternary elution system in Fig. 7, the three peaks would get even more crowded. However, if the preparative sample size changes to a very small analytical-scale sample size, baseline separation with a smaller separation time is still possible as demonstrated in Fig. 8. Fig. 8 has the same parameters as Fig. 7, except β=0.99, corresponding to a shell volume fraction of 0.03, and a dimensionless sample pulse size of 0.01, 100 times smaller than that used in Figs. 5–7. The very large β value means that such cored beads are similar to non-porous beads with a very small loading capacity that is suitable only for fast analytical separations, because a sizeable preparative-scale load would simply overwhelm the very limited retention time range due to the much larger band sizes.

Figs. 5–7 clearly indicate the existence of an optimal β value for the preparative-scale separation of a three-component system. This optimal β value depended on mass transfer and isotherm conditions of a specific system and the sample size. Optimization of β means achieving a proper balance between sharper peaks and sufficient retention time differences.

In Fig. 5, the peak areas for the three peaks (from left to right) for β=0.5 cored beads were numerically integrated from the concentration profiles and they were found to be 1.0001, 1.0001, and 0.9996, respectively. They matched extremely well with the sample pulse size of one in dimensionless time used in the simulation. This is another partial indication of the accuracy of the numerical methods used in this work.

4. Conclusions

In frontal analysis, the increase of core radius fraction for cored beads reduced the column hold-up capacity, resulting in earlier and sharper breakthrough curves. This corresponded to a shorter retention time and a sharper peak in isocratic elution. Peak concentrating effect was observed in a simulated ternary isocratic elution with baseline separation. Computer simulation pointed to an optimal cored radius fraction that provided faster baseline

separation in multicomponent isocratic elution than both fully porous and non-porous (two extreme cases) for a particular system. This means that a series of cored beads with various core radius fractions may be offered in a product line for different mass transfer and isotherm (i.e., thermodynamic) conditions in order to achieve faster baseline separation. The general rate model presented in this work can be a useful tool for product design and selection of cored beads. The ternary system used in this work is an example of successful optimization. It does not indicate that all systems can be optimized to achieve baseline separations. Some system may have excessive sample sizes or very limited retention time differences to start with.

The personal computer (PC) based software is free for academic research from the corresponding author. All the simulated chromatograms can be readily reproduced using the software and the parameters listed in Table 1 and mentioned in the discussion. Computer CPU times for each simulated chromatogram in this work ranged from a fraction of a second to a few seconds on a single-core Pentium-4 3.0 GHz PC.

Nomenclature

A	orthogonal collocation matrix for first-order derivative as defined by Finlayson (1980)
a	Langmuir isotherm parameter (dimensionless), bC^{∞}
B	orthogonal collocation matrix for second-order derivative as defined by Finlayson (1980)
b	Langmuir isotherm parameter (mol^{-1} L)
Bi	Biot number for mass transfer, $kR_p/(\varepsilon_p D_p)$
CA	dimensionless column hold-up area for a breakthrough curve
C_0	feed concentration of a solute, max $\{C_f(t)\}$ (mol L^{-1})
C_b	concentration of a solute in the bulk-fluid phase (mol L^{-1})
c_b	C_b/C_0
$C_f(t)$	feed concentration time profile of an eluite (mol L^{-1})
C_p	concentration of a solute in the stagnant-fluid phase inside particle macropores (mol L^{-1})
C^{∞}	adsorption saturation capacity based on unit volume of porous particle skeleton (mol L^{-1})
C_p^*	concentration of a solute in the solid phase of particles based on unit volume of particle skeleton (mol L^{-1})
c_p	C_p/C_0
c_p^*	C_p^*/C_0
D_b	axial dispersion coefficient ($\mathrm{m}^2\ \mathrm{s}^{-1}$)
D_p	effective diffusivity in particle macropores ($\mathrm{m}^2\ \mathrm{s}^{-1}$)
i	subscript for eluite (species) i in a multicomponent mixture
k	film mass transfer coefficient ($\mathrm{m\ s}^{-1}$)
L	column length (m)
N	number of interior collocation points
N_e	number of quadratic finite elements
N_s	number of components
Pe_L	Peclet number of axial dispersion for a solute, vL/D_b
R	radial coordinate for a particle in cylindrical coordinate system (m)
R_{core}	radius of the inert core (m)
R_p	particle radius (m)
r	dimensionless radial coordinate, R/R_p
t	Dimensional time ($t=0$ is the moment a sample enters a column) (s)
v	interstitial velocity ($\mathrm{m\ s}^{-1}$), $\mathrm{LQ}/(V_b\varepsilon_b)$
Z	column axial coordinate in cylindrical coordinate system (m)
z	Z/L

Greek Letters

β	core radius fraction, R_{core}/R_p
γ	dimensionless radial coordinate, $(r-\beta)/(1-\beta)$
ε_b	bed voidage (aka bed void fraction)
ε_p	particle porosity (gel pore portion of the cored beads)
η	dimensionless mass transfer parameter, $\varepsilon_p D_p L/(R_p^2 v)$
ξ	dimensionless mass transfer parameter, $3Bi\,\eta(1-\varepsilon_b)/\varepsilon_b$
τ	dimensionless time, vt/L

Acknowledgment

The model and the software in this work were developed with financial support from Millipore Corporation in a project that was completed in Jan. 2006. We thank Dr. Ganesh Iyer for his helpful comments.

References

Brown, P.N., Byrne, G.D., Hindmarsh, A.C., 1989. VODE: a variable coefficient ODE solver. SIAM Journal on Scientific and Statistical Computing 10, 1038–1051.

Cabootera, D., Fanigliulob, A., Bellazzi, G., Allieri, B., Rottigni, A., Desmeta, G., 2010. Relationship between the particle size distribution of commercial fully porous and superficially porous high-performance liquid chromatography column packings and their chromatographic performance. Journal of Chromatography A 1217, 7074–7081.

Coutinho, F.M.B., Carvalho, D.L., La Torre Aponte, M.L., Barbosa, C.C.R., 2001. Pellicular ion exchange resins based on divinylbenzene and 2-vinylpyridine. Polymer 42, 43–48.

Ding, Y., Sun, Y., 2005. Small-sized dense magnetic pellicular support for magnetically stabilized fluidized bed adsorption of protein. Chemical Engineering Science 60, 917–924.

Fanigliulo, A., Cabooter, D., Bellazzi, G., Tramarin, D., Allieri, B., Rottigni, A., Desmet, G., 2010. Comparison of performance of high performance liquid chromatography columns packed with superficially and fully porous 2.5 μm particles using kinetic plots. Journal of Separation Science 33, 3655–3665.

Fekete, S., Ganzler, K., Fekete, J., 2010. Facts and myths about columns packed with sub-3 μm and sub-2 μm particles. Journal of Pharmaceutical and Biomedical Analysis 51, 56–64.

Finlayson, B.A., 1980. Nonlinear Analysis in Chemical Engineering. McGraw-Hill, New York, p. 77, p. 97..

Greibrokk, T., 2004. The contributions of Csaba Horvth to liquid chromatography. Journal of Separation Science 27, 1249–1254.

Gu, T., Tsai, G.-J., Tsao, G.T., Ladisch, M.R., 1990. Displacement effect in multicomponent chromatography. AIChE Journal 36, 1156–1162.

Gu, T., 1995. Mathematical Modeling and Scale-up of Liquid Chromatography, Berlin-New York. Springer, pp. 14–15, p. 27.

Horvath, C.G., Preiss, B.A., Lipsky, S.R., 1967. Fast liquid chromatography: an investigation of operating parameters and the separation of nucleotides on pellicular ion exchangers. Analytical Chemistry 39, 1422–1428.

Kaczmarski, K., Guiochon, G., 2007. Modeling of the mass-transfer kinetics in chromatographic columns packed with shell and pellicular particles. Analytical Chemistry 79, 4648–4656.

Kirkland, J.J., 1969. Controlled surface porosity supports for high speed gas and liquid chromatography. Analytical Chemistry 41, 218–220.

Kirkland, J.J., Truszkowski, F.A., Dilks, C.H., Engel, G.S., 2000. Superficially porous silica microspheres for fast high-performance liquid chromatography of macromolecules. Journal of Chromatography A 890, 3–13.

Kiss, I., Bacskay, I., Kilár, F., Felinger, A., 2010. Comparison of the mass transfer in totally porous and superficially porous stationary phases in liquid chromatography. Analytical and Bioanalytical Chemistry 397, 1307–1314.

Lee, W.-C., 1997. Protein separation using non-porous sorbents. Journal of Chromatography B 699, 29–45.

Li, P., Yu, J., Xiu, G., Rodrigues, A.E., 2010. A strategy for tailored design of efficient and low-pressure drop packed column chromatography. AIChE Journal 56, 3091–3098.

Manchon, N., Arrigo, M.D., Garcia-Lafuente, A., Guillamon, E., Villares, A., Ramos, A., Martinez, J.A., Rostagno, M.A., 2010. Fast analysis of isoflavones by high-performance liquid chromatography using a column packed with fused-core particles. Talanta 82, 1986–1994.

Misak, N.Z., 1993. Langmuir isotherm and its application in ion-exchange reactions. Reactive Polymers 21, 53–64.

Miyabe, K., 2008. Evaluation of chromatographic performance of various packing materials having different structural characteristics as stationary phase for fast high performance liquid chromatography by new moment equations. Journal of Chromatography A 1183, 49–64.

Ning, J., Kong, F.Z., Li, D.H., Du, Y.Z., 1998. Preparation of monodisperse agglomerated pellicular anion-exchange resins compatible with high-performance liquid chromatography solvents for ion chromatography. Journal of Chromatography A 793, 193–197.

Palsson, E., Gustavsson, P.E., Larsson, P.O., 2000. Pellicular expanded bed matrix suitable for high flow rates. Journal of Chromatography A 878, 17–25.

Pesek, J.J., Frost, J.H., 1973. Adsorption as a mechanism for separation of nonionic solutes by pellicular ion exchange chromatography. Analytical Chemistry 45, 1762–1765.

Pietrogrande, M.C., Dondi, F., Ciogli, A., Gasparrini, F., Piccin, A., Serafini, M., 2010. Characterization of new types of stationary phases for fast and ultra-fast liquid chromatography by signal processing based on AutoCovariance function: a case study of application to *Passiflora incarnata* L. extract separations. Journal of Chromatography A 1217, 4355–4364.

Rissler, R., 2000. Separation of polyesters by gradient reversed-phase high-performance liquid chromatography on a 1.5 μm non-porous column. Journal of Chromatography A 871, 243–258.

Wang, C., Soice, N.P.., Ramaswamy, S., Gagnon, B.A., Umana, J., Cotoni, K.A., Bian, N., Cheng, K.-S.C., 2007. Cored anion-exchange chromatography media for antibody flow-through purification. Journal of Chromatography A 1155, 74–84.

Wang, X.L., Barber, W.E., Carr, P.W., 2006. A practical approach to maximizing peak capacity by using long columns packed with pellicular stationary phases for proteomic research. Journal of Chromatography A 1107, 139–151.

Xiang, Y.Q., Yan, B.W., McNeff, C.V., Carr, P.W., Lee, M.L., 2003. Synthesis of micron diameter polybutadiene-encapsulated non-porous zirconia particles for ultrahigh pressure liquid chromatography. Journal of Chromatography A 1002, 71–78.

Yang, G.L., Hu, Z.D., 1996. Universal theoretical moment expressions for elution and frontal chromatography of pellicular ion exchange resins. Reactive & Functional Polymers 31, 25–29.

Zhou, X., Shi, Q-H, Bai, S., Sun, Y., 2004. Dense pellicular agarose-glass beads for expanded bed application: fabrication and characterization for effective protein adsorption. Biochemical Engineering Journal 18, 81–88.

Zhou, X., Sun, Y., Liu, Z., 2007. Superporous pellicular agarose–glass composite particle for protein adsorption. Biochemical Engineering Journal 34, 99–106.